Angular Subtraction at LIGO Livingston Observatory Interim #1

Brian Seymour,[1] Marie Kasprzack,[2] Arnaud Pele,[2] and Adam Mullavey[2]
[1] *LIGO SURF Student, University of Virginia*
[2] *LIGO SURF Mentor, LIGO Livingston Observatory*
(Dated: July 14, 2017)

I. Introduction

In 1916 gravitational waves were predicted by Albert Einstein as a byproduct of his general theory of relativity which describes the relation between spacetime and matter. Just as accelerating charges emit light in classical electrodynamics, gravitational waves are emitted by accelerating masses. Gravitational waves travel at the speed of light in vacuum but, contrary to the latter, they are not obstructed by matter [1].

Gravitational waves will lead to new physics and astrophysics to examine the universe in complement to the existing information such as electromagnetic radiation and particles. Since gravity is much weaker than the other four fundamental forces, it is challenging to set up an experiment with gravity due to the large scale required to observe it. Thus, research in gravity is done by observing astrophysical signals around us, and gravitational waves will provide a new way to see more direct influences of the effects of gravity [2]. Additionally, predictions of general relativity can be compared to the gravitational wave data to test the validity limits of the theory. Lastly, gravitational wave astronomy will open a myriad of astronomical data, from examining black holes to probing past the cosmic microwave background. The cosmic microwave background may include a gravitational wave background, which would be evidence for inflation.

Laser Interferometer Gravitational-Wave Observatory (LIGO) is a collaboration dedicated to finding gravitational waves. It consists of two main facilities in Livingston, Louisiana and Hanford, Washington. These facilities detect gravitational waves with an optical system based on the interferometer developed by Michelson and Morley. Each observatory consists of a Michelson interferometer with 4 kilometer arms which measure the deformation of space produced by gravitational wave by looking for intensity variations in the interference pattern. It contains Fabry-Perot cavities which allows the light to bounce along the arms about 280 times. It uses light recycling to increase the power of a 25W laser into a 100KW laser in the arms. The laser also travels through a vacuum and dampens out environmental vibrations both actively and passively. The main optics are suspended with four stages of pendulums to passively isolate them from ground motion, and is kept at its operating point by active control through a plethora of feedback and feedforward techniques.

After LIGO searched for gravitational waves in the 2000's with no clear detections. Afterwards, the detectors were upgraded via the Advanced LIGO project.

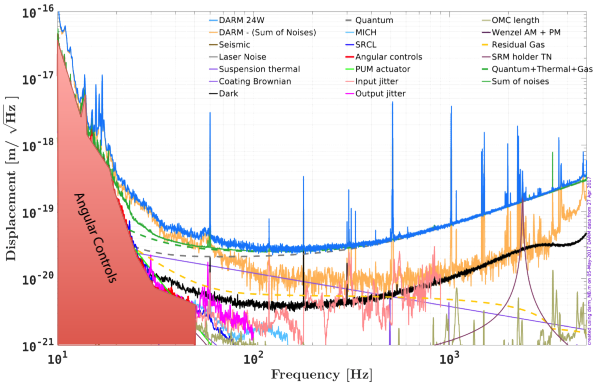

FIG. 1. Notice the sharp uptick in angular noise 25Hz, where it quickly becomes the dominant source of noise at 10Hz.

With these improvements, in September 2015, LIGO detected the first gravitational wave, and they had a second detection in December 2015 [3] [4]. Both of these detections were due to binary black hole system rotating and then combining.

In order to keep the mirrors stable, LIGO uses an active alignment sensing and control system (ASC) to reduce the mirror's angular motion [5]. Currently, the low frequency sensitivity (10-15 Hz) of the LIGO Livingston instrument is limited by the angular control feedback loops. To reduce the noise in this frequency band, the angular noise to DARM coupling should be reduced below 1/10th of the design sensitivity at that frequency [5].

II. Work Done

- Gained familiarity with techniques used by reading references provided. This includes gaining more knowledge in the following:
  - interferometric gravitational wave detector workings
  - Control systems
  - Digital signal processing and data analysis (specifically random data analysis)
  - Wiener filtering and spectral subtraction
  - Better knowledge of optics to better understand angular sensing and control
- Learned about LIGO instrument and focus on angular control systems and incorporate knowledge

gained from the readings with feedback and feed-forward control systems.

- Learned about WFS, ADS, Optical Lever, and other ASC systems in LIGO.
- Practiced some discrete fast fourier transform and power spectrum problems with Matlab.
- Learned about the tools to take necessary online data. Measurements templates will be created with the online LIGO tool DTT or generated with Matlab depending on the progress.
- Worked on a model for change in cavity length in the Fabry-Perot Cavity with a Gaussian beam.
- Used the hard-soft basis to in the model to remove cross couplings in length change.

III. Change in Cavity Length in Fabry-Perot Cavity

III.1. Beam Spot Motion Approach to Angular Noise

In the interferometer cavity, angular rotations can create noise by coupling to cavity length. This is because the beam is not centered the mirror's center of rotation, and this distance is called static beam spot offset. When the mirror rotates slightly, this causes a change in cavity length (eq 1). The equation depends on frequency however, and for the Fourier transform of equation 1, both the beam spot offset and mirror angle depend on frequency. The convolution can be approximated as in equation 2 [5].

$$\Delta l(t) = d_{spot}(t) \times \theta_{mirror}(t) \tag{1}$$

$$\begin{aligned} \Delta L(f) &= D_{spot}(f) * \Theta_{mirror}(f) \\ &\approx d_{spot}^{RMS} \times \Theta_{mirror}(f) + \theta_{mirror}^{RMS} \times D_{spot}(f) \end{aligned} \tag{2}$$

III.2. Cavity Misalignments

A laser beam in the Fabry-Perot cavity is shifted away due to angular misalignment in the cavity mirrors. The length of the cavity that the light beam travels is changed. This manuscript will describe methods to deduce both the beam position displacement and corresponding length changes as shown in Figure 2. The resulting change in cavity length from both arms contributes to the noise seen by the DARM channel.

A beam in the Fabry-Perot cavity must go through the two centers of curvature of the mirrors. So, when the mirrors rotate, their centers of curvature change. This causes the beam line to change. We have two x and two z coordinates from the centers of curvature here to define the line, and we will use these to find the points that the beam hits the mirrors.

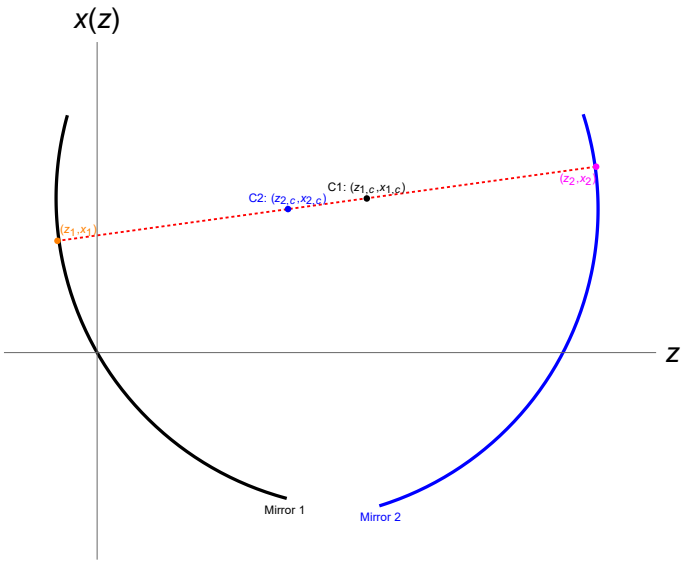

FIG. 2. This figure shows the setup of the mirrors. The points in the middle are the locations of the center of curvatures of each mirror. The points on the mirror are coordinates that this paper desires to find.

III.3. Change in Cavity Length

If a beam hits the mirrors at points (z_1, x_1) and (z_2, x_2), the change in cavity length, ΔL, can be found. Note, the angles and center of curvature coordinates are implicitly in the variables of equation 3. The initial cavity length before perturbation is L.

$$\Delta L = L' - L = \sqrt{(x_2 - x_1)^2 + (z_2 - z_1)^2} - L \tag{3}$$

III.4. Beam Reflection Location in Fabry-Perot Cavity

The left mirror is the input test mass (ITM) in this paper and the right mirror is the end test mass (ETM). For notation simplicity, the ITM angle is θ_2 (CCW convention) and the ETM angle is θ_1 (CW convention) with both measuring the angular misalignment. Let x be the height of the beam at position z horizontally. The following constants are the locations of the center of curvature of mirror 1 and 2.

$$\begin{cases} z_{1c} = R_1 \cos(\theta_1) \\ x_{1c} = R_1 \sin(\theta_1) \\ z_{2c} = L - R_2 \cos(\theta_2) \\ x_{2c} = R_2 \sin(\theta_2) \end{cases} \tag{4}$$

The beam line pictured in red must go through the two centers of curvature. Therefore the slope, m, can be obtained.

$$\begin{aligned} m &= \frac{x_{1c} - x_{2c}}{z_{1c} - z_{2c}} \\ &= \frac{R_1 \sin(\theta_1) - R_2 \sin(\theta_2)}{R_1 \cos(\theta_1) + R_2 \cos(\theta_2) - L} \end{aligned} \tag{5}$$

The beam path is given in equation 6. The equations for the mirror curves are in equations 7 and 8.

$$\begin{cases} x_{beam}(z) = x_{1c} + m(z - z_{1c}) & (6) \\ R_1^2 = (x(z) - x_{1c})^2 + (z - z_{1c})^2 & (7) \\ R_2^2 = (x(z) - x_{2c})^2 + (z - z_{2c})^2 & (8) \end{cases}$$

What remains to be found is the points of intersection of the beam and the mirrors. Substituting $x_{beam}(z)$ into the mirror equations, the solution emerges in equation 12:

$$R_1^2 = (x_{1c} + m(z - z_{1c}) - x_{1c})^2 + (z - z_{1c})^2 \tag{9}$$
$$R_1^2 = (m(z - z_{1c}))^2 + (z - z_{1c})^2 \tag{10}$$
$$R_1^2 = (m^2 + 1)(z - z_{1c})^2 \tag{11}$$
$$z = z_{1c} \pm \frac{R_1}{\sqrt{m^2 + 1}} \tag{12}$$

By symmetry the second intersection can be found. The extraneous roots are removed since the angle is less than $\pi/2$ radians (eq (13) and (14)). The coordinates of the beam spot are $(z_1, x(z_1))$ and $(z_2, x(z_2))$. Thus ΔL can be determined from these coordinates when placed in (3).

$$z_1 = z_{1c} - \frac{R_1}{\sqrt{m^2 + 1}} \tag{13}$$
$$z_2 = z_{2c} + \frac{R_2}{\sqrt{m^2 + 1}} \tag{14}$$

III.5. Change in Cavity Length to the Second Order

A second order approximation for equation (3) can be found around the point $(\theta_1, \theta_2) = (0, 0)$ now that the values in equations (13) and (14) have been found. This is shown in equation 15. A discussion about how this was found is through Mathematica is located in appendix A. The g factors are unitless constants; in real system their values are: $g_1 = g_{etm} = -.7794$ and $g_2 = g_{itm} = -1.0655$ [6].

$$\begin{aligned} \Delta L \approx \Delta L_{2nd} &= \frac{L}{2(1 - g_1 g_2)}(g_2\theta_1^2 + 2\theta_1\theta_2 + g_1\theta_2^2) \\ g_i &= 1 - \frac{L}{R_i} \end{aligned} \tag{15}$$

IV. Hard and Soft Basis

IV.1. Motivation of Hard-Soft Basis from Radiation Pressure

When the beam is not aligned with the cavity axis, the radiation pressure of the beam exerts a torque on the mirrors. This reduces the pendulum restoring torque by the mirror suspension which can increase misalignment. Radiation pressure torque depends on the beam spot displacement. Equation (17) shows the value of the radiation pressure torque as a function of angle by linking it with equation (16) [6].

$$\vec{x}_{sa} = \begin{bmatrix} x_{1,sa} \\ x_{2,sa} \end{bmatrix} = \frac{L}{1 - g_1 g_2} \begin{bmatrix} g_2 & 1 \\ 1 & g_1 \end{bmatrix} \begin{bmatrix} \theta_1 \\ \theta_2 \end{bmatrix} \tag{16}$$

$$\vec{\tau}_{opt} = \frac{2P}{c} \begin{bmatrix} x_1 \\ x_2 \end{bmatrix} = -\boldsymbol{K_{opt}} \begin{bmatrix} \theta_1 \\ \theta_2 \end{bmatrix} \tag{17}$$

Equation (17) gives a differential equation for torque. The hard-soft basis is one that diagonalizes the $\boldsymbol{K_{opt}}$ matrix in order to solve the differential equation (18) [6]. Equation (19) is the change of basis matrix for the diagonalization [5].

$$\vec{\tau}_{ext} = \boldsymbol{I}\ddot{\vec{\theta}} + \boldsymbol{\gamma}\dot{\vec{\theta}} + (\boldsymbol{\kappa_p} + \boldsymbol{K_{opt}})\,\vec{\theta} \tag{18}$$

$$\boldsymbol{S} = \begin{bmatrix} 1 & r \\ r & -1 \end{bmatrix} \tag{19}$$
$$r = \frac{2}{(g_2 - g_1) + \sqrt{(g_1 - g_2)^2 + 4}} \tag{20}$$

As laser power increases in the cavity, eigenvectors of the $\boldsymbol{K_{opt}}$ have a negative restoring spring constant. As radiation pressure increases, the eigenvalue for the spring constant k_{soft} decreases in equation (21). Thus, control systems designed to mitigate this are used to keep the mirror alignment at its operating point.

$$\boldsymbol{S} \times \boldsymbol{K_{opt}} \times \boldsymbol{S^{-1}} = \begin{bmatrix} k_{soft} & 0 \\ 0 & k_{hard} \end{bmatrix} \tag{21}$$

This radiation pressure example has motivated an interesting soft-hard basis with nice properties. The hard mode represents rotation of the cavity axis, and the soft mode represents a vertical displacement of the cavity axis. Figure 3 shows this.

IV.2. The Cavity Length Change Approximation in Hard-Soft Basis

Cavity length change equation (15) can be converted into the hard-soft basis. Just as it diagonalized the radiation pressure matrix, it removes the cross terms from

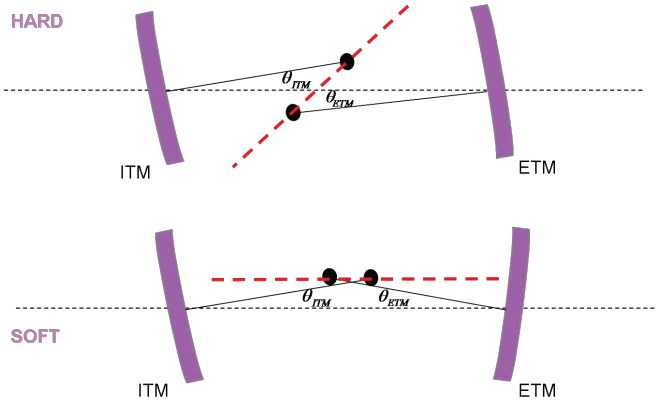

FIG. 3. This picture shows what the soft-hard basis angles look like in the cavity. This figure originated in [5].

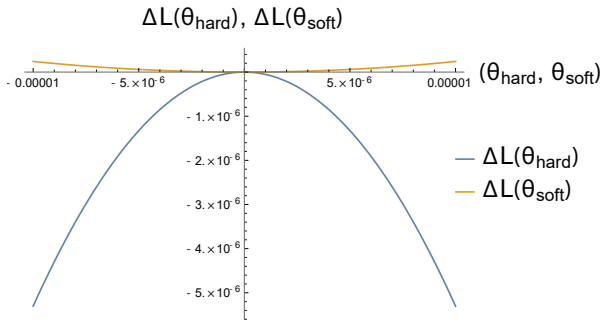

FIG. 4. This figure shows how the cavity length changes as a function of the soft and hard modes.

the cavity length change equation. The result is below in equation (22). The second equation includes the numerical values for the LIGO Livingston interferometer, which is calculated by using g factors and the initial cavity length.

$$\Delta L_{2nd} = \frac{L}{2(1-g_1g_2)}\Big[\theta^2_{soft}(g_1r^2+2r+g_2) + \theta^2_{hard}(g_2r^2-2r+g_1)\Big] \quad (22)$$

$$\Delta L_{2nd} = 2407.84\,\theta^2_{soft} - 53043.2\,\theta^2_{hard} \quad (23)$$

This equation for hard and soft modes is shown in is shown in figure 4.

V. Future Inquiry

Now that I have a model which explains how the mirror angles couple to the cavity length, I plan to take measurements of the interferometer and compare. I am currently working with my mentors to figure out the best sensors to take data from. I also would like to examine my model more in the frequency domain in order to better compare with much of the existing data which is in the frequency domain. If there is time left, I also would like to working on reducing DC motion on the pendulum length to test mass angle through by taking data and working on a feed forward model.

A. Exact Results from Mathematica

This appendix has the exact values of the coordinates found in section III.4. It also has the full equation for ΔL that was found. Equation (A1) was used in Mathematica to find the Taylor series in equation (15) from section III.5.

$$\begin{aligned}\Delta L = \mathrm{Abs}\Bigg(& L\sqrt{\frac{(R_1\sin(\theta_1)-R_2\sin(\theta_2))^2}{(-L+R_1\cos(\theta_1)+R_2\cos(\theta_2))^2}+1} - R_1\cos(\theta_1)\sqrt{\frac{(R_1\sin(\theta_1)-R_2\sin(\theta_2))^2}{(-L+R_1\cos(\theta_1)+R_2\cos(\theta_2))^2}+1} \\ & - R_2\cos(\theta_2)\sqrt{\frac{(R_1\sin(\theta_1)-R_2\sin(\theta_2))^2}{(-L+R_1\cos(\theta_1)+R_2\cos(\theta_2))^2}+1} + R_1 + R_2\Bigg) - L\end{aligned} \tag{A1}$$

$$z_1 = R_1\left(\cos(\theta_1) - \frac{1}{\sqrt{\frac{(R_1\sin(\theta_1)-R_2\sin(\theta_2))^2}{(-L+R_1\cos(\theta_1)+R_2\cos(\theta_2))^2}+1}}\right) \tag{A2}$$

$$x_1 = R_1\left(\sin(\theta_1) + \frac{R_1\sin(\theta_1)-R_2\sin(\theta_2)}{(L-R_1\cos(\theta_1)-R_2\cos(\theta_2))\sqrt{\frac{(R_1\sin(\theta_1)-R_2\sin(\theta_2))^2}{(-L+R_1\cos(\theta_1)+R_2\cos(\theta_2))^2}+1}}\right) \tag{A3}$$

$$z_2 = \frac{R_2}{\sqrt{\frac{(R_1\sin(\theta_1)-R_2\sin(\theta_2))^2}{(-L+R_1\cos(\theta_1)+R_2\cos(\theta_2))^2}+1}} + L - R_2\cos(\theta_2) \tag{A4}$$

$$\begin{aligned}x_2 = {} & R_1\sin(\theta_1) + \frac{((R_1\sin(\theta_1)-R_2\sin(\theta_2))}{-L+R_1\cos(\theta_1)+R_2\cos(\theta_2)} \\ & \times\left(\frac{R_2}{\sqrt{\frac{(R_1\sin(\theta_1)-R_2\sin(\theta_2))^2}{(-L+R_1\cos(\theta_1)+R_2\cos(\theta_2))^2}+1}} + L - R_1\cos(\theta_1) - R_2\cos(\theta_2)\right)\end{aligned} \tag{A5}$$

[1] R. Kinney, A. Weinstein, O. Miyakawa, and R. Ward. Development of Noise Budgets for the LIGO 40m IFO SURF 2005. June 2005.

[2] Peter Saulson. *Fundamentals of Interferometric Gravitational Wave Detectors*. World Scientific, 1994.

[3] B. P. Abbott, R. Abbott, T. D. Abbott, M. R. Abernathy, F. Acernese, K. Ackley, C. Adams, T. Adams, P. Addesso, R. X. Adhikari, and et al. Observation of Gravitational Waves from a Binary Black Hole Merger. *Physical Review Letters*, 116(6):061102, February 2016.

[4] B. P. Abbott, R. Abbott, T. D. Abbott, M. R. Abernathy, F. Acernese, K. Ackley, C. Adams, T. Adams, P. Addesso, R. X. Adhikari, and et al. GW151226: Observation of Gravitational Waves from a 22-Solar-Mass Binary Black Hole Coalescence. *Physical Review Letters*, 116(24):241103, June 2016.

[5] Lisa Barsotti and Matt Evans. Modeling of alignment sensing and control for advanced ligo. *LIGO Document Control Center*, 2009. LIGO-T0900511-v4.

[6] Katherine Laird Dooley. *Design and performance of high laser power interferometers for gravitational-wave detection*. University of Florida, 2011. LIGO-P1100125-v1.